CENTER FOR
APPLIED ENERGY
RESEARCH

3572 Iron Works Pike
Lexington, KY 40511-8433
FAX: 606-257-0220

DOE/PC/90056--T4

DE92 015654

QUARTERLY PROGRESS REPORT

FOR JANUARY-MARCH, 1992

TECHNOLOGY DEVELOPMENT FOR IRON FISCHER-TROPSCH CATALYSTS

#DE-AC22-91PC90056

P.I.: B. H. Davis

Begin Date: 12/18/90

End Date: 12/17/93

UK
An Equal Opportunity/
Affirmative Action University

SYNTHESIS OF SINGLE PHASE α-Fe, Fe_3C AND Fe_7C_3 NANO-PARTICLES BY CO_2 LASER PYROLYSIS TECHNIQUE

P. C. Eklund and X. X. Bi

Center for Applied Energy Research
University of Kentucky
3572 Iron Works Pike
Lexington, KY 40511

Synthesis of Single Phase α-Fe, Fe_3C and Fe_7C_3 Nano-particles by CO_2 Laser Pyrolysis Technique

I. Introduction

Iron-containing catalysts have been known to be useful in assisting the Fischer-Tropsch(FT) reaction for synthesizing hydrocarbons[1, 2]. However, it has been well recognized that iron catalysts are not stable during the reaction but converted into iron carbides. It is thus important to understand the role of the iron carbides in the catalytic reaction of the FT-synthesis[3]. It has been found difficult to produce iron carbide nano-particles as a single phase, because iron carbide phases are only metastable under 1 atm pressure[4]. Iron carbide bulk particles prepared so far are often contaminated with metallic iron, iron oxides and free carbon. In this study, we investigate the synthesis of iron carbide nano-particles using CO_2 laser pyrolysis technique. We show that this technique is successful in synthesizing α-Fe, Fe_3C and Fe_7C_3 nano-particles in their single phase with sizes in the range of 5 - 20nm. In particular, we have produced for the first time the Fe_7C_3 which has been known to exist but unable to be produced as a single phase. Furthermore, it is interesting that Fe_5C_2 which has carbon and iron ratio between Fe_3C and Fe_7C_3, is not seen in any run of our synthesis.

Fe_3C, known as "cementite", is the most stable phase among the known iron carbides, and in bulk form has been studied extensively for many years[1, 2, 5]. Another well studied carbide phase is Fe_5C_2(Hagg carbide)[5] frequently found in the FT-synthesis[6][1]. In contrast, much less attention have been given to Fe_7C_3, primarily due to the difficulty in producing this carbides as a single phase. This phase converts easily into cementite at temperature ~600 ^{o}C[7]. Its crystal structure was identified as hexagonal[8], pseudo-hexagonal[9] and orthorhombic[10]. The controversy in the identification of the crystal structure of this phase has been reviewed by Yakel[5].

A number of methods of producing nano-particles, such as gas-phase synthesis, vacuum synthesis and cluster deposition have been explored and reviewed[11-13]. The technique concerned in this work is

CO_2 laser pyrolysis, which is a gas-phase synthesis method first proposed by Haggerty[14] and later applied by Exxon[15, 16] to the generation of Fe_3C particles for the Fischer-Trosch catalysis. Laser pyrolysis offers many advantages[14]. First of all, it is a clean process that permits reaction free of contamination from chamber walls. Secondly, the reaction volume is very small(30 mm^3) with a well defined reaction zone, which is important in precisely controlling the nucleation and growth rate. Thirdly, the application of a CO_2 laser allows the particle production to be a flexible process, suitable for producing many different kinds of particles with different sizes. In the past, it has been used by several groups for producing particles such as TiO_2, SiC and etc.[14-18].

In this investigation, we have characterized our nanoparticles by using XRD, TEM, ^{57}Fe Mossbauer and Raman scattering. The application of these techniques has allowed us to systematically study the chemical composition, structure, morphology and size distribution of the particles produced by CO_2 laser pyrolysis. The results of our studies have established the appropriate reaction conditions for making α-Fe, Fe_3C and Fe_7C_3 nano-phase particles.

II. Experiment

The laser pyrolysis system[14-18] used for producing iron carbide nanoparticles is shown in Fig. 1. The cell was built from a six–way stainless steel cross with a tubular diameter roughly 4 cm. The reactant gases, composed of $Fe(CO)_5$ vapor and C_2H_4, flow vertically out of the tip of a narrow stainless tube and intersect the horizontal infrared beam from a tunable CW CO_2 laser(Laser Photonics Model 150) capable of delivering 150 W of power on most of the ~80 output lines. The reactant gas mixture is heated in a small reaction zone, defined by the intersection of the laser beam(dia. ~0.2-3 mm at beam waist) and a gas stream. The energy coupling is realized by tuning the laser frequency to a strong rotational-vibrational absorption band of C_2H_4 at 940 cm^{-1}. The P20 CO_2 line is used for this purpose.

The reactant gases and associated particle growth were confined within the

reaction zone above the nozzle by a coaxial flow of Ar gas which passed through a larger tube concentric with the much smaller reactant gas tube(see Fig. 1). The laminar Ar flow maintained the flow of particulate in a well–collimated stream all the way to the particle trap. Ar gas is also introduced into the entrance and exit windows in such a way as to continually sweep any stray particles off the NaCl windows, as shown in Fig. 1. This is particularly important; without this precaution the window deterioration can be triggered by particle deposition. Two mass flow controllers(AGA Gas, Inc.) were used to establish steady gas flows of Ar to the windows and coaxial sheath. Another mass flow controller was used to regulate the flow of C_2H_4 (2–30 sccm) through a sintered Pyrex bubbler into the glass container of liquid $Fe(CO)_5$. The bubbler is needed to generate numerous very small bubbles which are more effective than the larger ones for picking up saturated $Fe(CO)_5$ vapor. The total pressure in the cell was controlled by adjusting a needle valve located between a rotary vacuum pump and the 6-way cross, balanced mainly by Ar gas used to protect the windows and shield the particles. To control the laser power density and the height of the reaction volume, a ZnSe lens was used to position the laser beam waist relative to reactant gas nozzle. The beam waist(i. e. minimum beam diameter) can be continuously translated by changing the distance between the center of the chamber and the lens.

Particles are collected in a Pyrex trap indicated in Fig. 1. Since most particles produced by this process are ferromagnetic in their bulk form, we have employed a magnetic field to trap the particles. The field is provided by a stack of permanent ferrite magnets placed beneath the trap as shown in Fig. 1. The teflon membrane filter (pore size of 200 nm) is intended as an auxiliary device to stop particles which escape the magnetic field. Without the magnetic field, the membrane filter may be clogged soon after the process begins and the steady flow of the particles and reactant gases is interrupted. In the stead state, a 3mm, well collimated stream of particles can be seen to drift up the center of the 1cm diameter glass tube connecting the 6-way cross and particle trap.

Subsequent to synthesis, the UFP's were extracted from the collection vessel in

an "as–synthesized" form, or in a passivated form. Most particles are pyrophoric as synthesized. Passivation entailed the use of a 4% or 10% O_2–in–He_2 flow for periods of several hours, and in some cases up to 24 hours, during which time a thermocouple was used to monitor the temperature of collected particles. XPS data showed that the oxidation was on the particle surface. The passivation gas flow rate is limited in order not to raise the particle temperature by more than 20 degree or a run away reaction occurs. and the Fe-carbides are converted into oxides in the trap. Thoroughly passivated particles should show no temperature change when concentrated oxygen(such as air) is introduced into the trap. However, particle agglomeration may prevent some particles from contacting with oxygen. So care must be exercised at this step. It has been observed that the particles ignite after two weeks in an ordinary sealed glass container.

III. Results

In this section, we will present the characterization result of synthesized small particles in the laser pyrolysis system described above. The phase identification of the nano-particles is performed mainly by XRD, TEM and Mossbauer techniques. Raman and EDS have been employed to study the existence of oxygen and amorphous carbon in the produced particles.

In Fig. 2, we show Mossbauer spectra at 12 K for bulk Fe_3C(Fig. 2a), which was obtained from 20–50 micron powder, and a particular UFP sample which is predominantly Fe_3C(Fig. 2b) with average particle size 15 nm. Plotted in Fig. 2c and Fig. 2d, are the corresponding XRD data for these two samples. XRD data were collected using Cu(Kα) radiation using a Phillips powder diffractometer. Note the insensitivity of the Mossbauer spectra to particle size, whereas the XRD spectra exhibit significant size dependent broadening. The solid line in Fig. 2a and 2b represents the calculated Mossbauer spectrum by fitting the data in the usual way, indicating a variable amount of α-Fe. Fe_3C is also ferromagnetic, so a six–line Mossbauer pattern is obtained for this phase which is actually the superposition of two individual six–line

patterns from each of the inequivalent Fe–sites. Both the bulk and UFP samples contain a minority phase (~10%) of α–Fe which has one Fe site. The resulted parameter values from the data fitting including the internal magnetic field, isomer shift and quadruple splitting are compared with the results of Le Caer et al.[3], showing a good agreement. The Mossbauer study on Fe_7C_3 particles will be given in a separate study[19].

In Fig. 3, we show a transmission electron microscope (TEM) image (Hitachi H-800-NA) of some of Fe_3C particles taken at a magnification of 100,000x. In this picture, we observe the lattice fringes of Fe_3C particle, and the fringes spacing is consistent with lattice constants of Fe_3C phase[20]. Also observed in this picture are lattice images of the particle coating consistent with a lattice constant 3.5 Å. This spacing is similar to d_{002} of pyrolytic carbon, and therefore gives direct evidence for a carbon coating. This identification is supported by Raman scattering results presented below. A scanning electron microscope (SEM; ETEC OMNISCAN) equipped with an energy dispersive spectrometer (EDS) was used to probe the particles for oxygen. The spatial resolution of the instrument was such that ~1000 particles were averaged simultaneously. EDS results showed no oxygen in the samples (sensitivity ~ 2%). We therefore conclude that oxygen added during passivation was present in monolayer or submonolayer amounts on the surface of the particles. XPS results on the particles indicated a surface stoichiometry Fe:C:O of ~ 1:1:2, i. e., an oxy-carbide surface.

Raman scattering experiments on selected "nanopowders" were carried out in the Brewsterangle, backscattering configuration (incident beam angle ~45° with respect to the surface normal and polarized in the plane of incidence). The beam was incident on a UFP powder surface produced by pressing gently the powder against a ferrite magnet substrate. This method of sample preparation resulted in a nearly specular sample surface. Dry N_2 gas was blown gently over the sample surface during the measurements to arrest or prevent the oxidation during the experiment. The room temperature spectra taken using the 4880 Å line of an Argon ion laser for Fe_3C nanoparticle samples are shown in Fig. 4. The dominant structure in the spectra is the

doublet with broad peaks centered at 1375 and 1580 cm^{-1}. This doublet is the well–known result for a disordered graphitic carbon, or pyrolytic carbon. The disorder in the hexagonal carbon network both broadens the graphitic peak seen at 1582 cm^{-1} in pristine graphite and generates a new peak in the vicinity of 1350-1380 cm^{-1}. The strength of the ~1360 cm^{-1} peak can be correlated with the disorder. Thus the carbon coating inferred from TEM lattice fringes was directly confirmed by Raman scattering. No X-ray evidence for carbon was found consistent with amorphous carbon as a thin graphitic coating on the particles. Raman active modes associated with the iron carbides were not observed, but are anticipated at lower frequency (200–600 cm^{-1}). Some iron oxides Raman peaks have been observed, as indicated in the Fig. 4. The peaks are confirmed by measuring the Raman scattering spectra on oxidized α-Fe particles produced in this apparatus. The Fe-carbide nanoparticles were found to be very sensitive to laser heating for powers as low as 30 mW. Unless N_2 gas is blown onto the particles, the particles exhibited immediate oxidation upon laser illumination. The sensitivity to this oxidation for the three phases of nanoparticles we have made decreases in the order α-Fe, Fe_3C and Fe_7C_3.

Shown in Fig. 5 are typical XRD results for three different phases of particles α–Fe, Fe_3C and Fe_7C_3 generated in our pyrolysis system using different reaction parameters. In this figure, solid dots represent experimental data whereas solid lines are calculated results using published powder diffraction intensity data[20]. The experimental diffraction data are fitted by a sum of Lorentzians, along with an exponential background. The calculated peak area is proportional to the published line intensity. A single line width for all Lorentzians is chosen to best fit the data by eye. A set of typical reaction parameters has been established for producing each of these phases, as given in Table I. The carbide phases Fe_3C and Fe_7C_3 are found nearly free of α-Fe and iron oxides which were the frequent source of contamination in the past. The signature of Fe_3O_4 in the XRD data of α-Fe comes from the passivation process(10% O_2 in He_2 at 200 torr), which is necessary to handle nano-size α-Fe in air. This passivation can be avoided if the nanoparticle trap were opened in a glove

box purged by N_2 gas. Clearly, the current pyrolysis system has demonstrated the capability of preparing different iron carbide particles as a single phase by simply choosing an appropriate set of reaction parameters.

Presented in Fig. 6 and Fig. 7 are the XRD results of several batches of Fe_3C and Fe_7C_3 particles with different particle sizes, as seen in the broadening of the diffracted peaks. The particle size indicated in the figure was estimated by using Debye-Scherer equation[21] for the peak near 58° for both Fe_3C and Fe_7C_3. Average particle sizes in the range of 6 - 17nm were obtained.

IV. Discussion.

We now discuss the connection between the phase and surface morphology of the nanoparticle powders and the synthesis reaction parameters. These parameters include: (1) reactant gas flow rate, (2) chamber pressure, (3) laser irradiation intensity, (4) power density and (5) nozzle diameter. Thus we have explored pockets in this 5-parameter space to discover what type of particles can be produced from the mixture of $Fe(CO)_5$ and C_2H_4. As proposed in the patent of this laser pyrolysis system in producing iron carbide materials[16], the basic chemical reaction evolves the decomposition of C_2H_4 and $Fe(CO)_5$ at high temperature sustained by laser energy. The iron carbide particles are formed while carbon and iron originated from C_2H_4 and $Fe(CO)_5$ recombined in the heated reaction zone. The usual contamination resulting from this process can be either free carbon or α–Fe, depending on the balance between Fe and carbon in the reactant gas.

Total pressure of the reaction chamber is one of the most important parameters which affect the properties of the particles, such as chemical composition and particle size. The effect of this parameter was explored by workers at Exxon [16] who found it controlled the amount of Fe in the produced particles. They did not carry out a qualitative analysis of the resulting phase mixture, however. Our studies revealed that $Fe(CO)_5$-C_2H_4 system is much more complex than suggested in their patent.

In the following discussion, the role of the chamber pressure in determining the

carbon and iron ratio of the reactant gas is presented. In Fig. 8, the pressures at several essential points in the reactor system are labeled, which will be convenient for the discussion. Shown schematically is the bubbler containing $Fe(CO)_5$ and the reaction chamber to the left. C_2H_4 gas first bubbles through the $Fe(CO)_5$ liquid, and then flows into the chamber with the $Fe(CO)_5$ vapor. Considering that a bubble with volume V and pressure P_B is formed at the bottom of $Fe(CO)_5$ liquid container, it is therefore reasonable to describe the bubble pressure P_B by

$$P_B=P_L+P_C$$

where P_L is the fluid pressure at the bottom of the liquid supplied by the $Fe(CO)_5$, and P_C is the pressure on the top of the liquid. In here, we assume that the pressure in the vapor above the $Fe(CO)_5$ liquid is approximately the same as the chamber pressure. In view of the fact that the bubble consists of C_2H_4 and $Fe(CO)_5$ vapor, we can also write the bubble pressure as

$$P_B=P_{C2H4}+P_{Fe(CO)5}$$

where P_{C2H4} and $P_{Fe(CO)5}$ are the partial pressures contributed by C_2H_4 and $Fe(CO)_5$, respectively. Clearly, the following equation holds

$$P_L+P_C=P_{C2H4}+P_{Fe(CO)5}$$

Since it is known that the vapor pressure of $Fe(CO)_5$ is 25 torr at room temperature, the C_2H_4 and $Fe(CO)_5$ pressure ratio is thus determined by

$$Ratio=P_{C2H4}/25=(P_L+P_C-25)/25 \quad (A)$$

where $P_L=\rho gh$, and ρ and h are the density and height of the $Fe(CO)_5$ liquid inside the glass container. In this apparatus, the height of the $Fe(CO)_5$ liquid is roughly 5 cm, from which we estimate P_L to be ~6 Torr. Comparing with 10^2 Torr of the total chamber pressure, which is normally used in the reaction process, P_L can certainly be neglected without introducing much error. From this formula, we see that C/Fe ratio is directly proportional to the chamber pressure P_C. This result can be used to guide the production of particles with different C/Fe ratio, such as FeC_0(α-Fe), Fe_3C and Fe_7C_3 which have C/Fe ratio as 0, 0.33 and 0.43. Indeed, the typical chamber pressures

under which these three phases of the particles were made are found to be 100 , 300 and 500 torr for FeC_0(α-Fe), Fe_3C and Fe_7C_3, as given in Table I.

It is necessary to realize that the above analysis is only approximate. Since the system is not in equilibrium, an accurate description of the process would require a dynamical model which include the effects caused by the gas flow. For example, the C_2H_4 bubble may expand when it flows onto the top of the $Fe(CO)_5$ liquid in stead of staying at the same size. Furthermore, the bubble may not be fully saturated by the $Fe(CO)_5$ vapor if the flow rate is too high, which makes the pressure of $Fe(CO)_5$ vapor less than the 25 torr as assumed.

C_2H_4 flow rate is another critical factor affecting the properties of the produced particles. Correlated closely with the flow rate is the velocity with which the reactant gas enter into the reaction zone. This velocity readily determines duration time of the particles staying in the reaction zone, which in turn controls the growth of the particle[14]. Shown in Fig. 9a, 9b and 9c are the XRD data for three batches of particles made under three different flow rate with other parameters fixed. These reaction parameters are provided in the table contained in the same figure. In correspondence with the flow rate, the samples are named as #1, #2 and #3 to the increasing flow rate values. First, we see a significant broadening of the diffraction peaks with the increased flow rate. This suggests the size reduction of the particles, which can be simply attributed to the shorter dwell time of the particles in the reaction zone as a result of their increased speed. A Second observation from this figure is the change of the XRD pattern when the flow rate is increased, indicative of the phase change of the particles. Comparing with sample #1, which has a phase mostly Fe_3C, sample #2 and #3 show progressively growing peaks associated with Fe_7C_3 in Fig. 9b and 9c, as marked by down arrows. Mossbauer results obtained on the same particles are given in Fig. 9c, 9d and 9e. The dots in the figure are experimental data taken at 12 K, while the solid lines are calculated using a set of parameters best fit to the data. Marked by down arrows in the Mossbauer data of Fig. 9d and 9e is the peak which grow with the increased C_2H_4 flow rate. We associate the appearance of this peak with

the structure change as seen in the XRD results for the three samples shown in Fig. 9a, 9b and 9c. In order to fit the whole Mossbauer spectrum of samples #2 and #3, we find it necessary to introduce a new set of parameters to describe the marked peaks appeared in the spectrum of sample #2 and #3, indicating the presence of third inequivalent site in the sample. The parameters relating to this site were found not matching with the ones of other known carbides. Since no Mossbauer data on Fe_7C_3 is available, we can only tentatively associate this growing feature as due to the formation of Fe_7C_3, which is demonstrated in the XRD results obtained from these three samples. A detailed Mossbauer study will be presented elsewhere[19].

The speed of the reactant gas molecules can also be altered by changing the opening area of the nozzle. Shown in Fig. 10 are the XRD data of two batches of particles produced by using a nozzle with different opening area, and the relevant parameters are included in the figure. It is evident from Fig. 10a that the sample made with the nozzle of large opening area is close to Fe_3C. The other sample made with the nozzle of smaller opening area shows the significant presence of Fe_7C_3 as seen in Fig. 10b. In this case, the C_2H_4 mass flow is kept at a constant by the mass flow controller. The only possible outcome from the change of nozzle opening area is the change of the speed of the particles and reactant gas molecules.

Another reaction parameter evolved in this process is the laser intensity, which has shown a strong influence on the chemical composition of the particles. This influence has been utilized to generate particles of different phases. Shown in Fig. 11 are the XRD spectrum of four batches of particles made with successively increased laser intensity while the other reaction parameters were held fixed. A transformation from Fe_7C_3 phase to α–Fe phase with increased laser intensity can be seen from the figure, along with the signature of small amount of Fe_3C. The appearance of a-Fe is illustrated in Fig. 11(e)-(h) by monitoring the growth of the diffraction peak around 2θ~65°, along with the collapse of Fe_7C_3 carbide phase indicated by the group of peaks centered at 45°. Assuming the reaction temperature is directly proportional to the laser intensity, we identify this phase change as due to the increased temperature

in the hot reaction zone. A similar change has also been observed in in situ XRD temperature studies performed on Fe_7C_3 particles in a atmosphere of He_2. Two possible mechanisms may be attributed to be responsible for this transformation as described in the following. Fe_7C_3 has been known to be a metastable phase which may convert into the more stable phase Fe_3C when heated up to 600 °C[8, 22]. Further heating may disassociate the Fe_3C phase into α–Fe and carbon due to the metastable properties of Fe_3C. Therefore, excess heat during the reaction favors the formation of Fe_3C, or the disassociation of Fe_3C. This two-step process is supported by the presence of small amount of Fe_3C phase along with the α–Fe particles as shown in Fig. 11b, 11c and 11d, which may indicate that a transformation from Fe_7C_3 to Fe_3C occurs prior to the evaporation of carbon. However, another possibility is the direct evaporation of carbon in Fe_7C_3 phase due to the fast laser heating, whereas the presence of Fe_3C is caused by the reaction in some low temperature region induced by the inhomogeneity of laser beam across the reaction zone. We are as yet unable to distinguish these two process, and further studies are under going to clarify this situation.

The laser beam width above the reactant gas nozzle has been found to have a great impact on the particle sizes. The narrower beam width usually results in smaller particles due to the short dwell time of the particles in the reaction zone. The wider beam, on the other hand, may produce larger size particles due to the prolonged growing time of the particles in the reaction zone. However, this lengthened time in the reaction zone may give rise to another effect. That is, the chemical composition of the particles may be altered under the long time laser heating. This effect has been shown in Fig. 12, in which we plotted the XRD spectrum of two samples made with different laser beam width, as given in the figure. It is clear that the signatures of Fe_7C_3 seen in Fig. 12a nearly disappears when laser beam width is increased. This process is accompanied by a growth of diffraction intensity of α–Fe phase at 65°. We suggest that this may be due to the disassociation of Fe_7C_3 into α–Fe and carbon, similar to what we have observed when the laser intensity is increased. It should be noted, however,

that the study of the effect induced by the laser beam width is complicated by the fact that the adjustment of laser focusing also results in a change of the laser power density in the reaction zone as well as the heated reaction volume. To solve this problem, we need to measure the beam width by a microscope of a long working distance so that we can estimate the power density in the reaction zone, in order to keep it the same while we change the laser intensity. More studies are currently under way to understand the behavior of the particles on the variation of beam width.

Based on the above analysis, we can now discuss the appropriate reaction conditions for producing the particles with different phases. The current system has shown the capability to produce three kinds of particles, identified as Fe_3C and Fe_7C_3 and α-Fe with different sizes. The basic procedure and typical parameter setting are now described for each of these three phases.

i. α-Fe

In order to make pure phase α-Fe particles, we first need to adjust the reactant gas concentration to favor high vapors of $Fe(CO)_5$. This can be achieved by simply running the reaction under low chamber pressure as described previously. The α-Fe particle grows when $Fe(CO)_5$ is decomposed thermally into Fe plus CO in the reaction zone. However, the generation of pure α-Fe particles requires a low reactivity with C_2H_4 and CO, which may lead to the formation of a carbide phase. This can be accomplished by keeping the laser intensity just high enough to decompose the $Fe(CO)_5$. Thus, usually no flame can be observed in the reaction zone in this case. α-Fe particles obtained in this way are found to be extremely pyrophoric, and ignite immediately in air. The passivation for such particles should be carried out with extra precaution. It is recommended to leak the $5\%O_2$+$95\%He_2$ into the collecting trap very slowly so that no significant temperature rise can be observed. The particles obtained after the passivation were examined by XRD, and showed a large amount of Fe_3O_4 in the passivated particles, as shown in Fig. 5(a). Thus the passivation using oxygen is difficult to keep only on the particle surface.

ii. Fe_3C

The second phase that we have made in the process is Fe_3C, which is a well-known carbide material. Fe_3C particles can be made with a chamber pressure higher than that used in making α-Fe, so as to encourage contact with C_2H_4. In order to initiate a significant reaction between Fe and C_2H_4, higher laser intensities(I >30 W) is required. This reaction usually is found to be associated with a visible, but dim flame above the nozzle. Even the Fe_3C particles have been shown to be air sensitive, and, in many cases, pyrophoric. However, they are much less reactive than α–Fe. The remaining pyrophoric behavior of Fe_3C particles may be attributed to the following: (1) Fe_3C is co-produced with small amounts of α–Fe. The heat generated by this reaction is enough to initiate the oxidation process of Fe_3C to oxy-carbides. (2) The possibility of unsatisfied Fe sites on the Fe_3C particle surface. Most of our observation suggest (2) is more likely, since no oxides such as Fe_3O_4 have been detected by XRD. Surface oxides would not give rise to peaks in XRD scans.

iii. Fe_7C_3

Fe_7C_3 has been recognized as a less stable phase, and a transformation to Fe_3C occurs in the bulk when at 600 °C[8, 22]. Consistent with the requirement for higher carbon content, the generation of Fe_7C_3 particles needs an even higher chamber pressure than that used for producing Fe_3C. It has been shown previously that there are several parameters which may influence the particle size and composition: laser intensity, focusing(i. e. beam diameter at nozzle), flow rate of the reactant gas and nozzle diameter. A conclusion can be drawn from the discussion about these parameters regarding the generation of Fe_7C_3. That is, low temperatures and short duration times in the reaction zone are crucial for producing Fe_7C_3 particles. These conditions also prevent Fe_7C_3 particles from transforming into Fe_3C, as well as from further decomposing into α–Fe with a carbon surface. Different from Fe_3C, freshly made Fe_7C_3 particles are found to react with air. In most cases, no slow passivation is needed. This may be due to the fact that the particles are coated with a thicker unreacted carbon coating on the surface, since the reaction of making Fe_7C_3 often evolves high carbon content in the reactant gas. However, due to the possible

presence of Fe_3C or α-Fe as minority phases in Fe_7C_3 batches, we still recommend O_2 passivation.

V. Conclusion

In summary, we have investigated systematically the relation between the particle properties and reaction parameters for the synthesis of ultrafine iron-carbide particles by using CO_2 laser pyrolysis technique. We have produced three phases of particles α-Fe, Fe_3C and Fe_7C_3, with different particle sizes. In particular, Fe_7C_3 is first time produced in a pure phase(except for some possible carbon coating), and to our knowledge, no existing techniques are able to make this phase in its pure form. The availability of pure phase Fe_7C_3 makes it possible to further study the crystal structure which has not been well determined. A recipe of reaction parameters for making these particles has been obtained. Therefore, we have for the first time demonstrated that this technique is capable of generating two single phase iron carbide nano materials by simply changing the reaction parameters. Particles have been characterized by several techniques including Mossbauer, XRD, TEM , and Raman Scattering. The accomplishment of both generation and characterization of these nano-particles is necessary for the catalytic study to be carried out.

Table1 Typical reaction parameters to generate three phases particles.

	α-Fe	Fe_3C	Fe_7C_3
Laser Intensity(W)	30	50	54
Beam Width(mm)	1	1	0.2
Nozzle Diameter(mm)	1.7	0.8	0.8
Chamber Pressure(Torr)	100	300	500
C_2H_4 Flow Rate(sccm)	9	9	25

VI. References

1. J. A. Amelse, G. grynkewich, J. B. Butt, and L. H. Schwartz, J. Phys. Chem., 1981. **85**: p. 2484-2488.
2. J. W. Niemantsverdriet, A. M. van der Kraan, W. L van Dijk, and H. S. van der Baan, J. Phys. Chem., 1980. **84**: p. 3363-3370.
3. Cohen, R. L., *Applications of Mossbauer Spectroscopy*. ed. R.L. Cohen. 1976-1980, New York: Academic Press.
4. Hansen, M., *Constitution of Binary Alloys*. 1958, New York, Toronto, London: McGraw-Hill. 353.
5. Yakel, H. L., International Metals Reviews, 1985. **30**: p. 17.
6. J. Fournier, L. Carreiro, Y-T. Qian, S. Soled, R. Kershaw, K. Dwight, and A. Wold, J. Solid State Chem., 1985. **58**: p. 211.
7. Adock, H. C. Echstrom and W. A., J. Amer. Chem. Soc., 1950. **72**: p. 1042.
8. F. H. Herbstein, and J. A. Snyman, Inorg. Chem., 1964. **3**: p. 894.
9. K. W. Andrews, D. J. Dyson and S. R. Keown, *Interpretation of Electron Diffraction Patters*. 1971, London: Hill..
10. M. Audier, and et al., J. of Crystal Growth, 1983. **63**: p. 125-134.
11. MRS Bulletin, 1990. **XIV**: p. 12.
12. MRS Bulletin, 1990. **XV**: p. 1.
13. R. P. Andres, R. S. Averback, W. L. Brown, W. A. Goddard, III, A. Kaldor, S. G. Louie, M. Moscovits, P. S. Peercy, S. J. Riley, R. W. Siegel, F. Spaepen, and Y. Wang, J. Mater. Res., 1989. **4**: p. 704.
14. Haggerty, J. S., *Sinterable Powders from Laser-Driven Reactions*, in *Laser-induced Chemical Processes*, J.I. Steinfeld, Editor. 1981, Plenum Press: New York.
15. G. W. Rice, and et al., United States Patent, 1987. **4,659,681**.
16. R. A. Fiato, G. W. Rice, S. Miseo, and S. L. Soled, United States Patent, 1987. **4,637,753**.
17. G. W. Rice, and R. L. Woodin. *Applications of Lasers to Industrial*. in *SPIE*. 1984.
18. G. W. Rice, and R. L. Woodin, J. Am. Ceram. Soc., 1988. **71**: p. C181.

19. P. C. Eklund, Mossbauer Study on Fe_7C_3 particles, in preparation.

20. JCPDS, Powder Diffraction Data, 1990

21. Cullity, B. D., *Elements of X-Ray Diffraction*. 1967, Addison-Wesley Publishing Company, Inc.

22. H. C. Eckstrom, and W. A. Adcock, J. Am. Chem. Soc., 1950. **72**: p. 1042.

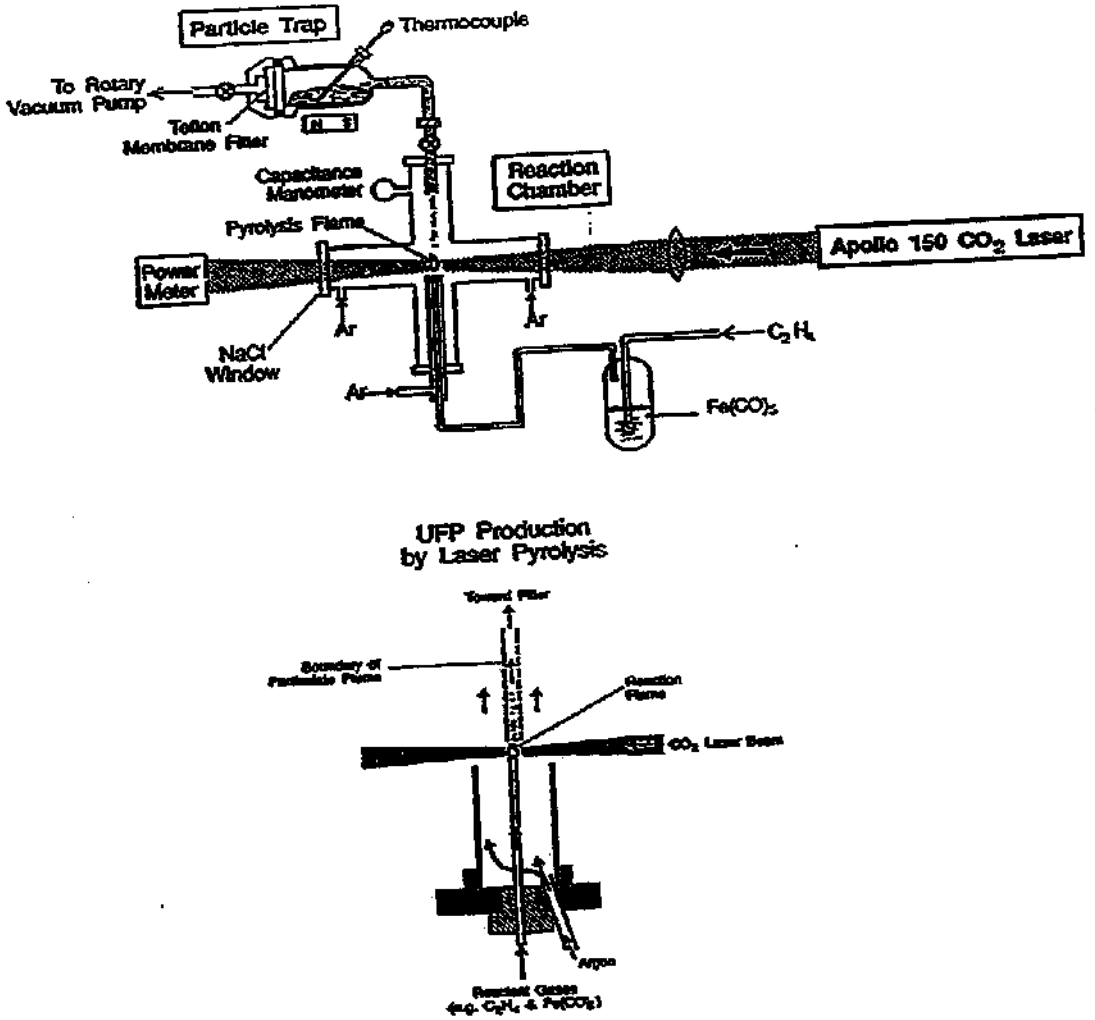

Fig. 1 Laser pyrolysis system for the generation of ultrafine Fe-carbide particles.

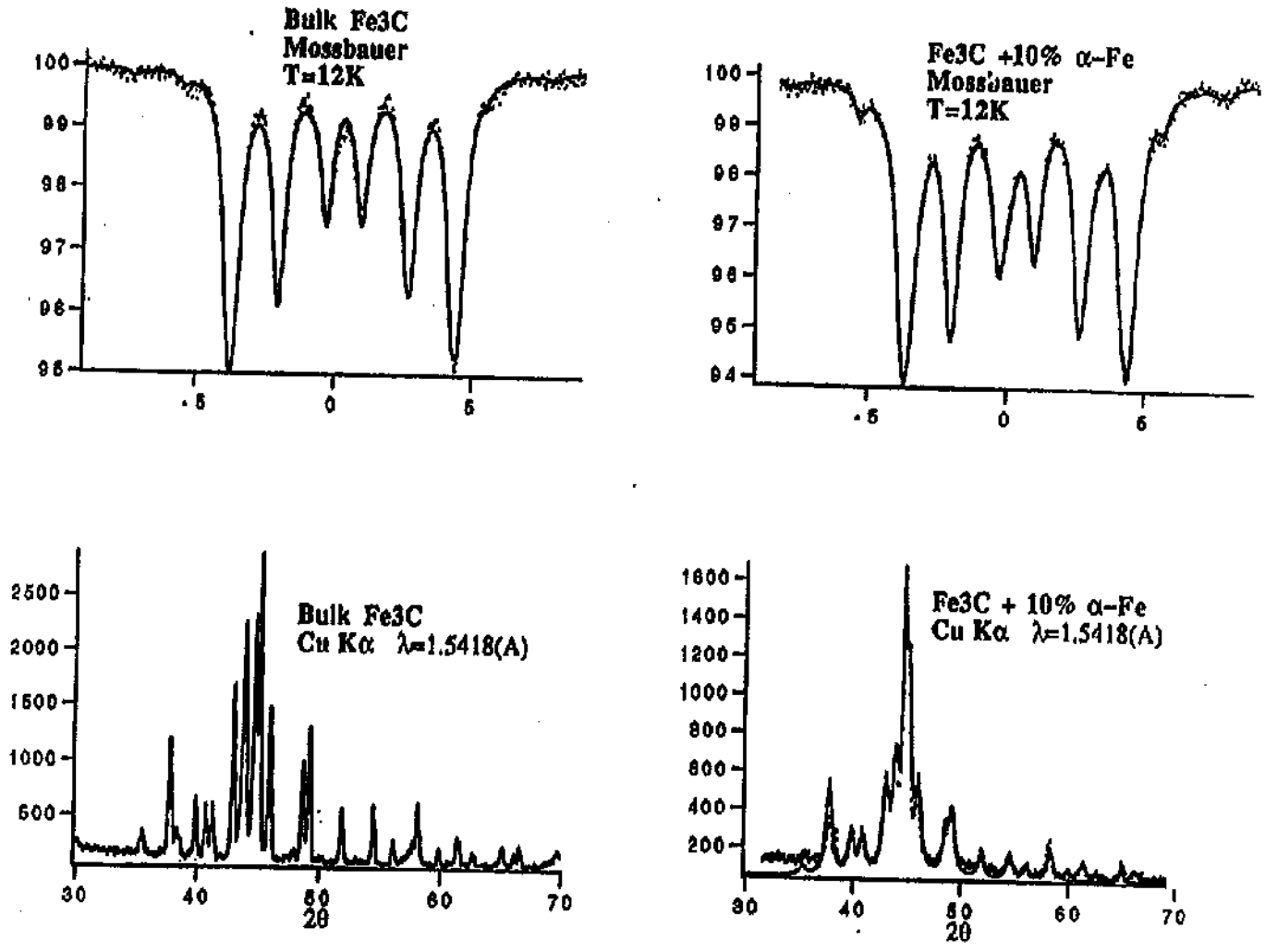

Fig. 2 XRD(lower panel) and Mossbauer(upper panel) results of Fe_3C particles with 10% α-Fe.

Fig. 3 TEM image of an isolated Fe_3C particle and carbon coating on the surface.

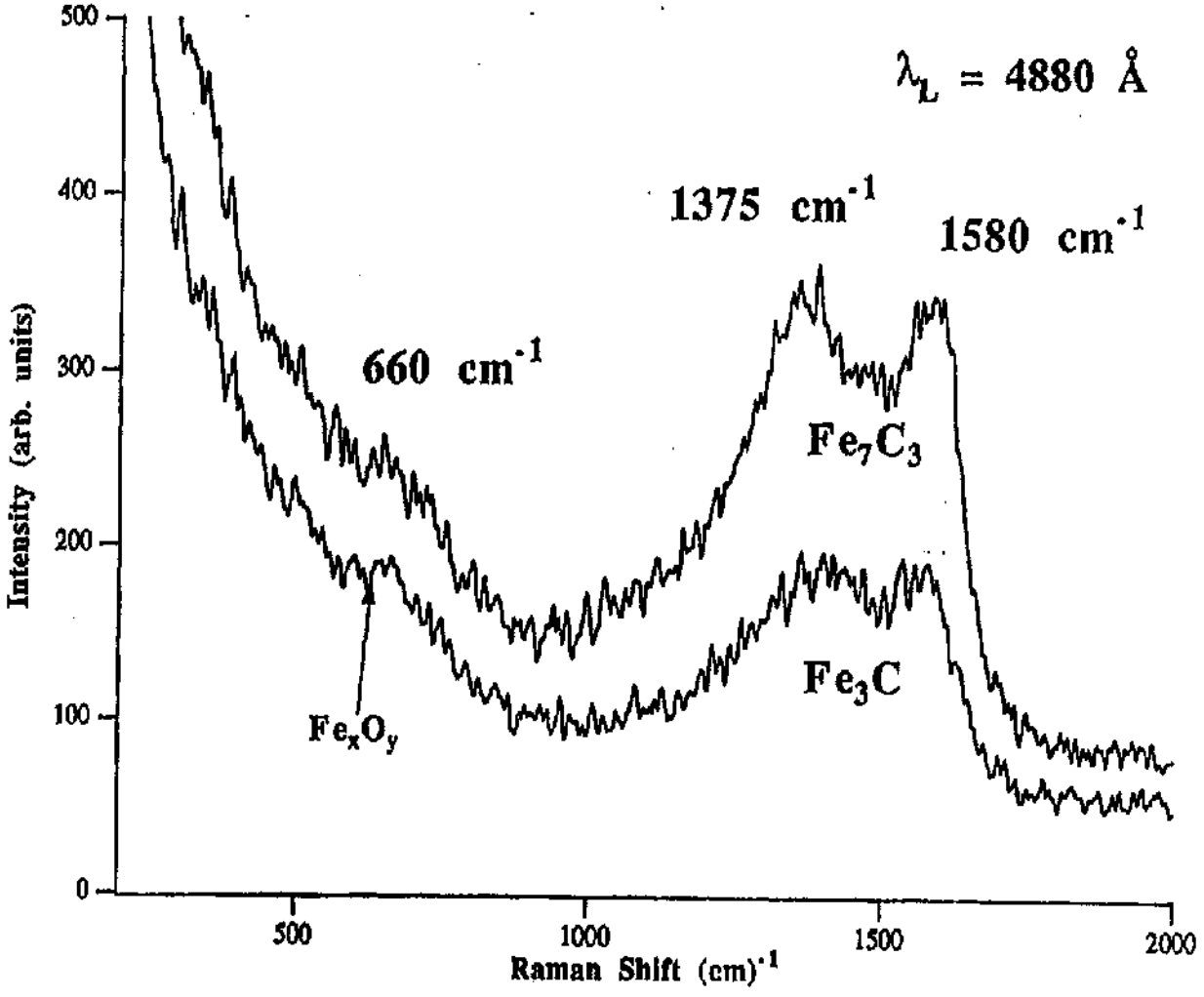

Fig. 4 Raman scattering of Fe_3C and Fe_7C_3 particles.

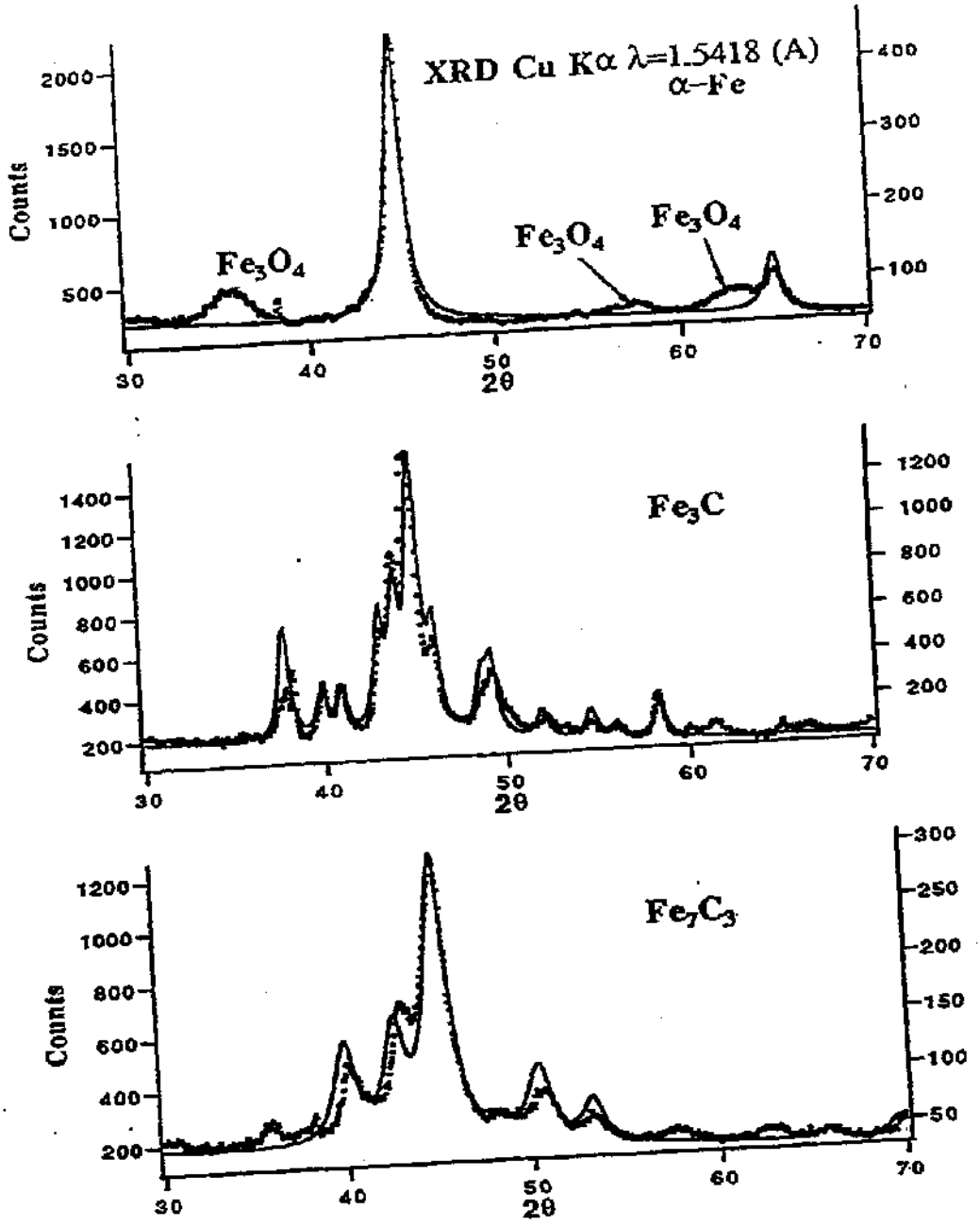

Fig. 5 Three pure phase nano-size particles , α-Fe, Fe_3C and Fe_7C_3. Solid lines are calculated using standard diffraction data for these three phases with an exponential background[90].

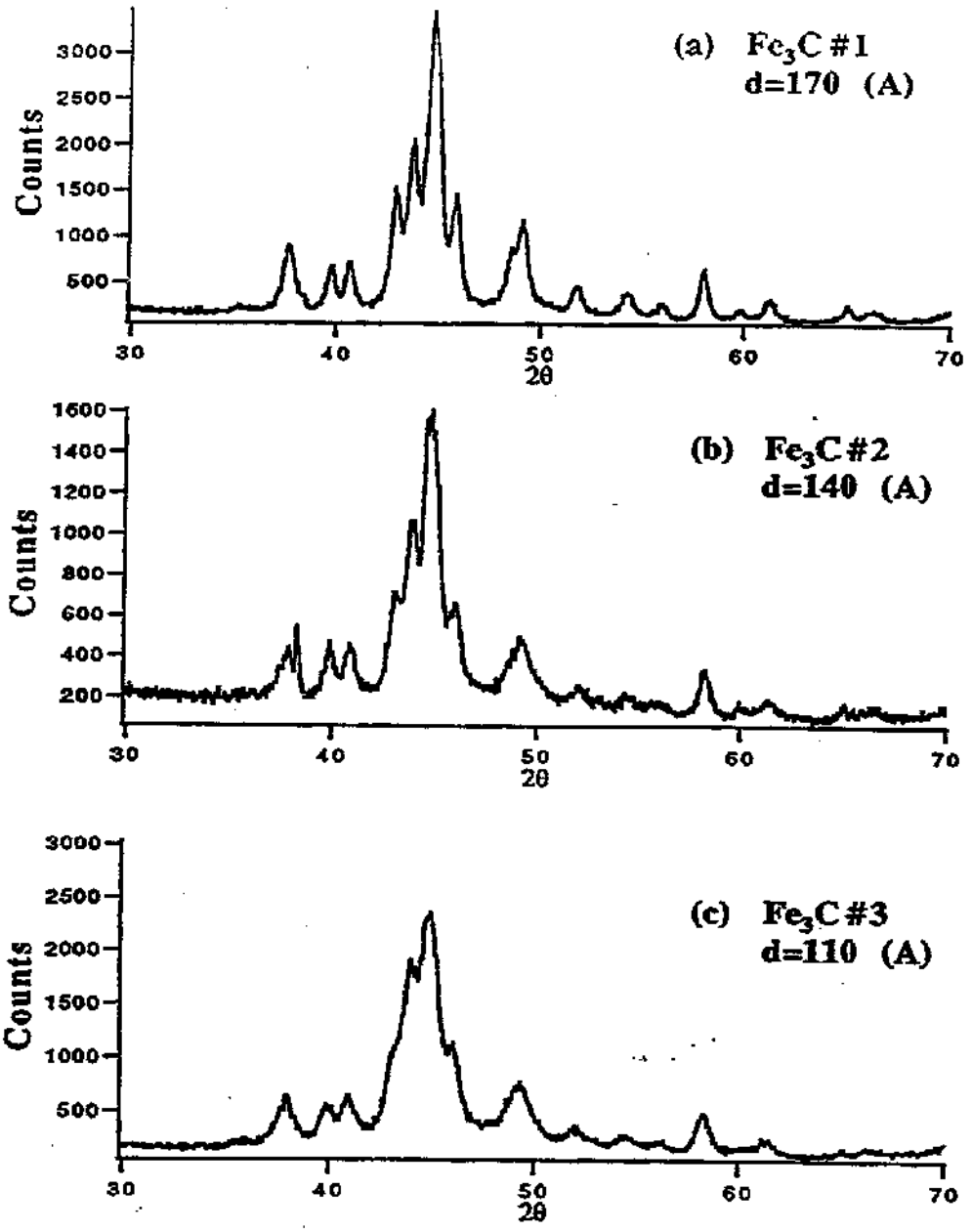

Fig. 6 XRD data of Fe_3C particles with three different particle size.

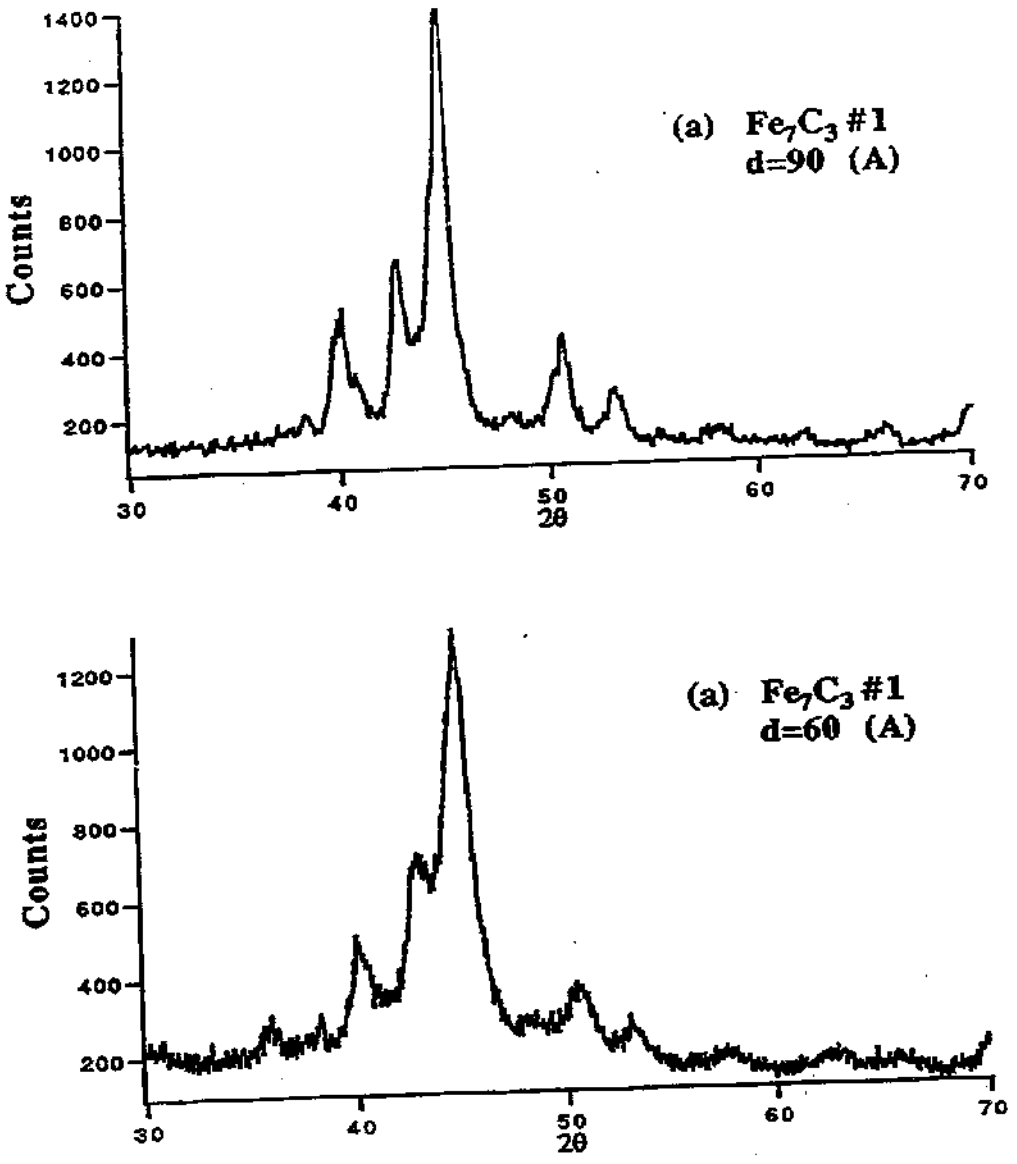

Fig. 7 XRD data of Fe_7C_3 particles with two different size.

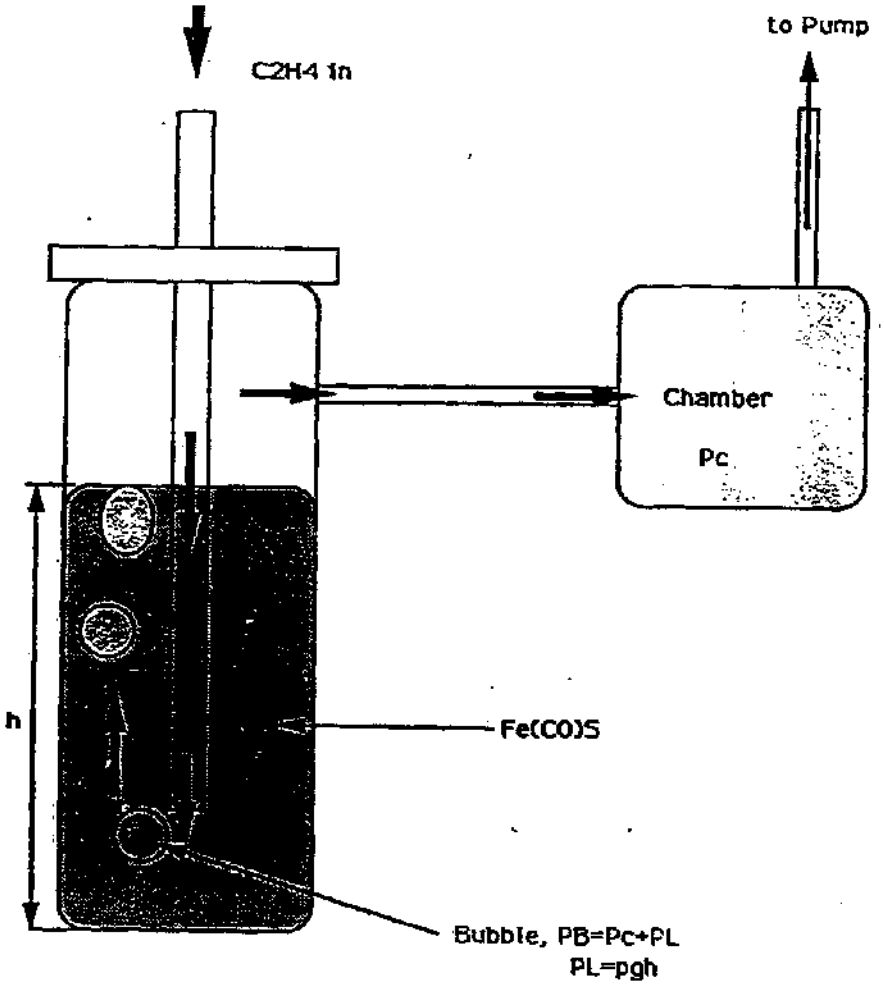

Fig. 8 A simplified schematics of C_2H_4 flow.

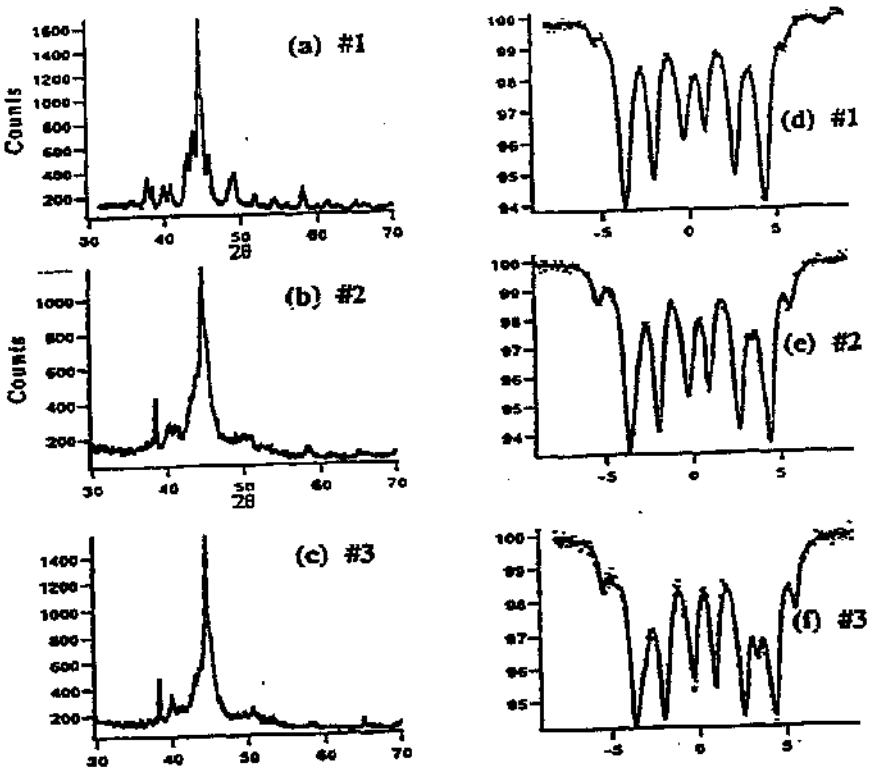

Point	Pressure_Torr	LaserInt_W	NozzleDia_mm	BeamWidth_mm
0	400	45	0.3	0.5
1	400	45	0.3	0.5
2	400	45	0.3	0.5

Point	FlowRate_sccm	SampleNo
0	9	1
1	27	2
2	33	3

C_2H_4 Flow Rate

Fig. 9 Flow rate induced structural phase change of particles.

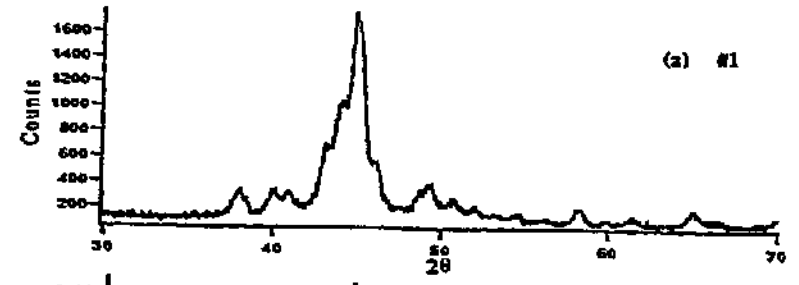

Flowrate_sccm	Pressure_Torr	LaserIntensity_W	BeamWidth_mm
100	100	60	2.2
100	100	60	2.2
100	100	60	2.2

NozzleArea_mm2	SampleNo
4	1
3	2
1.5	3

Nozzle Area

Fig. 10 Effect on the particle properties induced by reactant nozzle area.

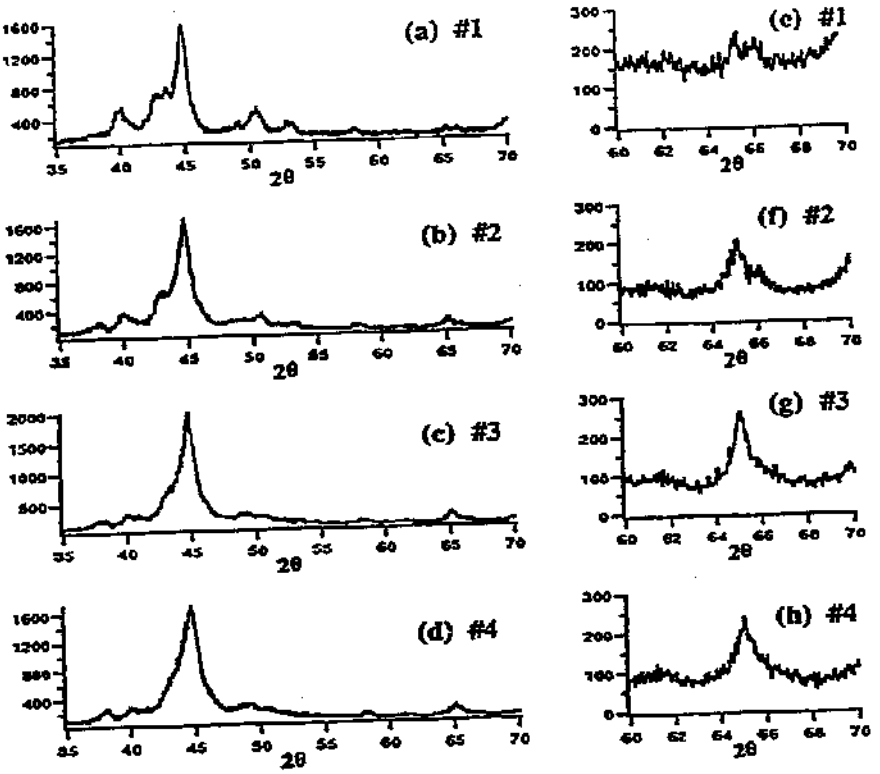

FlowRate_sccm	NozzArea_mm2	BeamWidth_mm	Pressure_torr
35	1.5	3	500
35	1.5	3	500
35	1.5	3	500
35	1.5	3	500

LaserInt_W	SampleNo
25	1
67	2
80	3
110	4

Laser Intensity

Fig. 11 Laser intensity induced particle phase change.

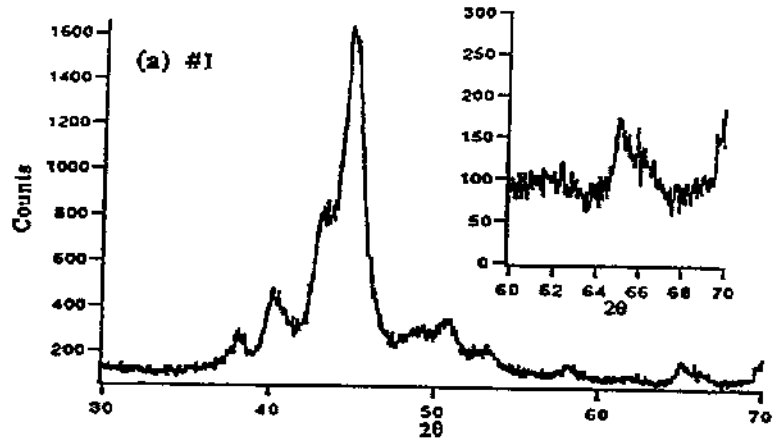

LaserInt_W	FlowRate_sccm	Pressure_Torr	NozzleArea_mm2
60	33	500	1.5
80	33	500	1.5

SampleNo	BeamWidth_mm
1	1
2	2.5

Laser Beam Width

Fig. 12 Effect on the particle properties induced by laser beam width.